electronic reprint

Journal of
Synchrotron Radiation
ISSN 0909-0495
Editors: **Å. Kvick, D. M. Mills and T. Ohta**

Diffractive imaging of nonperiodic materials with future coherent X-ray sources

Qun Shen, Ivan Bazarov and Pierre Thibault

Diffractive imaging of nonperiodic materials with future coherent X-ray sources

Qun Shen,[a,b]* Ivan Bazarov[c,a] and Pierre Thibault[d]

[a]Cornell High Energy Synchrotron Source, Wilson Laboratory, Cornell University, Ithaca, NY 14853, USA, [b]Department of Materials Science and Engineering, Cornell University, Ithaca, NY 14853, USA, [c]Laboratory of Elementary Particle Physics, Cornell University, Ithaca, NY 14853, USA, and [d]Laboratory of Atomic and Solid State Physics, Cornell University, Ithaca, NY 14853, USA. E-mail: qs11@cornell.edu

Coherent diffractive imaging using a coherent X-ray source promises to be a useful microscopic method for imaging noncrystalline objects at high spatial resolution. In this article a simple method to estimate the coherently scattered signal as a function of resolution is presented, and it is shown that the required X-ray flux or dose scales as the inverse third power of resolution for a specimen of constant volume and density. A simulated case study using the proposed energy-recovery linac source is also presented, which confirms the estimated flux requirement.

Keywords: coherent diffraction; diffractive imaging; iterative algorithm; oversampling; ERL; XFEL.

1. Introduction

In recent years there has been considerable interest in coherent diffractive imaging on noncrystalline specimens using coherent synchrotron radiation (Sayre, 1980, 2002; Miao *et al.*, 1999, 2002, 2003; Howells *et al.*, 2003; Williams *et al.*, 2003; He *et al.*, 2003). The activities are mainly motivated by two areas of desired advances in X-ray technology and science: X-ray imaging beyond the resolution limit set by X-ray optics, and development of next-generation intense synchrotron sources, such as X-ray free-electron lasers (XFELs) and energy-recovery linacs (ERLs), that have a high degree of transverse coherence (Arthur *et al.*, 2002; Gruner *et al.*, 2002; Shen *et al.*, 2003; Bilderback *et al.*, 2003).

The idea of coherent diffraction imaging, as proposed by Sayre (1980) in the early 1980s, is to determine the spatial distribution of electron density $\rho(\mathbf{r})$ in a noncrystalline specimen by measuring its far-field coherent X-ray diffraction pattern, which is essentially the Fourier transform $F(\mathbf{Q})$ of density $\rho(\mathbf{r})$, and retrieving the phases of the measured diffraction amplitudes. This methodology is very much analogous to X-ray crystallography, but with two important distinctions. First, the Fourier transform $F(\mathbf{Q})$ is a continuous function in reciprocal space for a noncrystalline specimen, as opposed to discrete Bragg peaks for a crystal. This allows the application of an iterative oversampling phasing algorithm (Fienup, 1982; Gershberg & Saxton, 1972; Miao *et al.*, 1999; Elser, 2003) for phase retrieval and structure determination. Second, the method requires an intense fully coherent X-ray beam incident on the specimen in order to preserve the phase information in the diffraction pattern and overcome the lack of periodicity in the specimen.

The requirement of an intense X-ray beam may cause substantial radiation damage to the sample, which would limit the applicability of the coherent diffraction imaging technique. In a recent study, Marchesini *et al.* (2003) applied a dose-fraction theorem (McEwen *et al.*, 1995) to coherent diffractive imaging and concluded that, owing to radiation damage to the sample and dose required to achieve a given resolution, the spatial resolution using this technique may be limited to $\sim$10 nm for biological specimens and to $\sim$1 nm for samples in materials science that are more radiation resistant. It has been proposed (Neutze *et al.*, 2000) that a possible way to overcome the radiation-damage limit is to use a single ultrashort pulse from an X-ray free-electron laser and record a diffraction pattern before a macromolecule Coulomb-explodes in the intense X-ray beam. However, the intensity from a single pulse may not be strong enough to record a high-resolution diffraction pattern. In this case many thousands of identical copies of each pattern need to be sorted from millions of diffraction patterns and added up to provide statistically significant signals at atomic resolution (Miao *et al.*, 2001).

In this article we address the basic questions of radiation dose requirement *versus* spatial resolution and radiation damage, using a straightforward first-principle calculation of coherently diffracted X-rays from a small fixed volume. Some of the derivations are elementary but are included nonetheless for completeness. The main focus here is to investigate the situation using a high-repetition-rate intense X-ray source such as the ERL, although a useful result for the XFEL is also presented. Various experimental parameters such as sample volume, detector pixel size and X-ray wavelength are discussed in the context of realistic experiments.

2. Coherent diffraction intensity

Suppose that a coherent X-ray beam with intensity I_0 is incident on a specimen of atom density n_0 and volume $V = L^3$, with L being the edge length of a cube (Fig. 1). According to the kinematic theory of X-ray scattering (Warren, 1969), the intensity $I(\mathbf{Q})$ scattered into a solid-angle pixel $\Delta\Omega$ at scattering angle 2θ is given by

$$I(\mathbf{Q}) = I_0 r_e^2 \left|F(\mathbf{Q})\right|^2 \Delta\Omega, \tag{1}$$

where $\mathbf{Q}$ is the momentum transfer with $Q = |\mathbf{Q}| = 4\pi \sin\theta/\lambda$, λ is the X-ray wavelength, $r_e = 2.818 \times 10^{-5}$ Å is the classical electron radius and $F(\mathbf{Q})$ is the scattering factor for the whole volume.

2.1. Ensemble-averaged coherent scattering

In order to obtain a realistic estimate of $I(\mathbf{Q})$, we first evaluate the coherent scattering amplitude $S(\mathbf{Q})$ from a single volume resolution element ΔV, and then calculate the ensemble-averaged scattering intensity by all volume elements in the sample. For convenience we choose to use a spherical volume element with radius R so that $\Delta V = 4\pi R^3/3$ and the scattering amplitude $S(\mathbf{Q})$ can be expressed as (Kirz *et al.*, 1995)

$$S(Q) = 4\pi n_0 R^3 f(Q) \frac{\sin QR - QR\cos QR}{(QR)^3}, \tag{2}$$

where $f(Q)$ is the scattering form factor of an average atom in the volume.

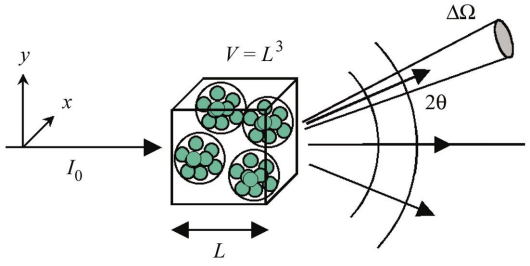

Figure 1
Schematic illustration of a coherent X-ray diffraction experiment.

Within sample volume V there are $N = V/\Delta V$ volume elements. In a coherent scattering experiment, when all volume elements scatter in-phase, $F(\mathbf{Q}) = NS(Q)$, and, when half of the volume elements scatter out-of-phase with respect to the other half, $F(\mathbf{Q}) = 0$ (assuming identical volume elements). This gives rise to a typical 'speckle' pattern. Without knowing the specific arrangements of volume elements in a sample, the best estimate of $F(\mathbf{Q})$ is given by the ensemble-averaged scattering amplitude represented by the root-mean-square value, $F(\mathbf{Q}) = N^{1/2}S(Q)$. Thus the average intensity in a solid-angle pixel $\Delta\Omega$ is

$$I(\mathbf{Q}) = I_0 r_e^2 N\left|S(Q)\right|^2 \Delta\Omega. \quad (3)$$

We note that this result is identical to that in conventional small-angle and wide-angle scattering. This is due to the fact that, as stated above, only an averaged coherent diffraction pattern can be evaluated without a given specific arrangement of all atoms in the sample. In fact, equation (3) represents the coherently scattered intensity averaged over all possible arrangements or ensembles of atoms. In §4 we will give an example of a specific diffraction pattern from a single ensemble of atoms, which would be completely different from the incoherent small-angle or wide-angle scattering results.

2.2. Angle-integrated coherent scattering

From equations (2) and (3) we can calculate the total scattered intensity integrated over all solid angles $0 \le \theta \le \pi/2$ and $0 \le \varphi \le 2\pi$,

$$I_{\rm scat} = \int\int I_0 r_e^2 N\left|S(Q)\right|^2 {\rm d}\Omega.$$

We now assume that a single sphere is our sample, $N = 1$ and $V = 4\pi R^3/3$. By noting that ${\rm d}\Omega = \sin 2\theta\, {\rm d}(2\theta)\, {\rm d}\varphi$ and defining $u = QR = 4\pi R\sin\theta/\lambda$, we obtain

$$I_{\rm scat} = 4I_0 r_e^2 \left(4\pi n_0 Z R^3\right)^2 \left(\frac{\lambda}{4\pi R}\right)^2 2\pi \int_0^{4\pi R/\lambda} \frac{(\sin u - u\cos u)^2}{u^5}\, {\rm d}u,$$

where n_0 is the atom density and we have omitted the angle dependence of $f(Q)$ for now. As given in the literature, the result of the above integral in the short-wavelength limit ($\lambda << R$) is (Kirz *et al.*, 1995)

$$I_{\rm scat} = I_0 r_e^2\, 2\pi n_0^2 \lambda^2 R^4 Z^2. \quad (4)$$

This result shows that the total integrated coherent scattering intensity from a sphere of radius R is proportional to $\lambda^2 R^4$, or its volume to the power 4/3 multiplied by the X-ray wavelength squared. However, in the long-wavelength limit, $4\pi R/\lambda << 1$, the integrand above can be approximated to the first two terms in its Taylor series, which yields

$$\begin{aligned} I_{\rm scat} &= I_0 r_e^2\, 4\pi n_0^2 Z^2 \left(16\pi^2/9\right) R^6 \\ &= I_0 r_e^2\, 4\pi n_0^2 Z^2 V^2, \end{aligned} \quad (5)$$

which is simply the scattered intensity of a single electron multiplied by the total number of electrons squared.

2.3. Coherent intensity at a given resolution

Our goal is to estimate the coherently scattered intensity at a given spatial resolution $d = 2R$. Thus $Q = 2\pi/d = \pi/R$. Setting $QR = \pi$ in (2) yields

$$S(\pi/R) = (4/\pi) n_0 R^3 f, \quad (6)$$

and (3) becomes

$$I(Q) = \left[1/\left(4\pi^2\right)\right] I_0 N r_e^2 n_0^2 f^2 d^6\, \Delta\Omega. \quad (7)$$

Equation (7) shows that $I(Q)$ is independent of X-ray wavelength λ for a fixed-solid-angle element $\Delta\Omega$. However, as shown in the following section, the requirement for an oversampled diffraction pattern would result in a λ^2-dependence in $\Delta\Omega$, which leads to a λ^2-dependence in $I(Q)$.

2.4. Oversampling in Fourier space

From the experimentalists' point of view, the oversampling of a coherent diffraction pattern is directly related to the angular resolution of a detector acceptance angle. For a two-dimensional area detector such as a charge-coupled device (CCD), its angular acceptance resolution is set by its pixel size Δx or Δy divided by its distance r from the sample. As illustrated in Fig. 2, if the longest length scale that exists in an object is L, then the detector angular resolution ΔQ in reciprocal space has to be finer than half of the corresponding spatial frequency $2\pi/L$, *i.e.* $\Delta Q \le \pi/L$, in order to make the interference fringes at that spatial frequency observable in a diffraction experiment. This means that the Fourier space needs to be *oversampled* by at least a factor of two compared with the highest spatial frequency $2\pi/L$.

It has been shown (Miao *et al.*, 1998) that the above statement is valid for two-dimensional (2D) and three-dimensional (3D) objects as well, and the overall minimum oversampling factor is always two

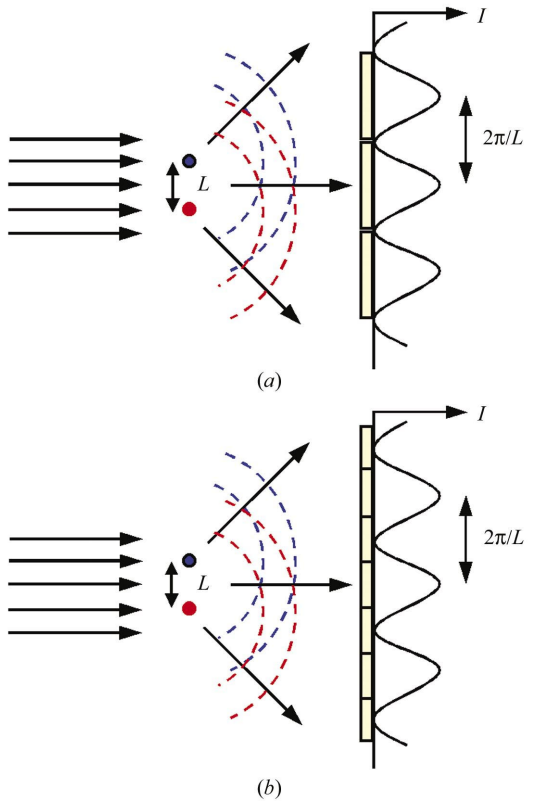

Figure 2
Illustration of the oversampling requirement from the point of view of detector angular resolution in a double-slit experiment. (*a*) The detector pixel size corresponds to an angular resolution that is equal to the highest spatial frequency $2\pi/L$, and no intensity modulations due to interference can be observed in this case. (*b*) Intensity variations can be observed if the detector pixel size corresponds to an angular width π/L and the pixels are spaced at π/L, which is half of the highest spatial frequency. Now the Fourier space is 'oversampled' by a factor of two compared with (*a*).

regardless of the dimensions. Thus the oversampling factor in each direction is

$$\Delta Q \leq \begin{cases} 2\pi/(2L), & \text{for the 1D case} \\ 2\pi/(2^{1/2}L), & \text{for the 2D case} \\ 2\pi/(2^{1/3}L), & \text{for the 3D case} \end{cases}. \quad (8)$$

In practice, a 3D diffraction pattern is always obtained by taking many 2D projections at different specimen orientations with respect to the incident beam. We note that the difference between 2D and 3D cases is only 12%, and we will use the more conservative 2D requirement for our estimation of scattered intensities.

Since the scattering signal in each solid-angle pixel is proportional to $\Delta\Omega$, it is preferable to use the largest $\Delta\Omega$ permitted, as given in (8). Using $Q = 4\pi \sin\theta/\lambda$, we obtain

$$\begin{aligned} \Delta Q_x &= [(4\pi \cos\theta)/\lambda]\Delta\theta = [(2\pi \cos\theta)/\lambda]\Delta(2\theta), \\ \Delta Q_y &= (2\pi/\lambda)\Delta\varphi, \end{aligned} \quad (9)$$

and the solid-angle element is thus (using the 2D case)

$$\Delta\Omega = \Delta(2\theta)\Delta\varphi = \left(\frac{\lambda}{2\pi}\right)^2 \frac{\Delta Q_x \Delta Q_y}{\cos\theta} = \frac{\lambda^2}{2L^2 \cos\theta}. \quad (10)$$

As an example, for $\lambda = 1.5$ Å, $L = 1000$ Å and $\theta \simeq 0$, we have $\Delta\Omega = 1.5^2/(2 \times 1000^2) = (1.06 \text{ mrad})^2$. For a CCD located at 100 mm from the sample, oversampling requires a pixel size no greater than 106 µm × 106 µm, which is very reasonable in practice. It is also interesting to note that the maximum solid angle scales with $1/\cos\theta$, so that the oversampling requirement becomes more relaxed in the radial direction at higher scattering angles.

3. Scaling law and dose requirement

In this section we derive a final expression for coherent diffraction intensity, examine how it scales with various parameters, and estimate the flux and dose requirements for achieving a certain diffraction resolution.

3.1. Scaling with diffraction resolution

Inserting (10) into (7), we obtain

$$I(Q) = \frac{I_0}{8\pi^2 L^2} N r_e^2 \lambda^2 n_0^2 f^2 d^6, \quad (11)$$

for N/L^2 = a constant. In the case of a constant volume $V = L^3$ with atom density n_0, $N = V/\Delta V$ for the number of volume elements, we have

$$I(Q) = \frac{I_0}{8\pi^2 L^2} \frac{V}{(4/3)\pi R^3} r_e^2 \lambda^2 n_0^2 f^2 d^6,$$

or

$$I(Q) = \frac{3I_0}{4\pi^3} L r_e^2 \lambda^2 n_0^2 f^2 d^3 \quad (12)$$

for $V = L^3$ = a constant. Equation (12) may be compared with the recent result of Howells *et al.* (2003) if the sample thickness L scales with the desired resolution d, *i.e.* $L \propto d$,

$$I(Q) = \frac{3I_0}{4\pi^3} r_e^2 \lambda^2 n_0^2 f^2 d^4, \quad (13)$$

for $V = L^2 d$.

It is apparent from (11)–(13) that the coherently diffracted intensity $I(Q)$ has different scaling behavior with diffraction resolution d under different circumstances. For a constant 2D-projected particle density N/L^2, the scattered intensity $I(Q)$ scales as d^6, as given by (11). For a constant volume with fixed atom density n_0, intensity $I(Q) \propto d^3$, as given by (12). Finally, for a sample volume $V = L^2 d$, intensity $I(Q) \propto d^4$, as given by (13). In an experiment on a single given specimen, (12) applies and the coherently scattered signal scales with d^3 and is proportional to sample thickness L. A summary of these scaling laws is given by

$$I(Q) \propto \begin{cases} d^6, & \text{if 2D, } N/\text{area} = \text{a constant} \\ d^4, & \text{if 2D, } V = \text{area} \times d \\ d^3, & \text{if 3D, } V = \text{a constant} \end{cases}. \quad (14)$$

We note that (12), or the 3D case in (14), represents the scaling law of an individual 2D-projected diffraction pattern from a specimen of a constant 3D volume.

3.2. X-ray wavelength dependence

In addition to the resolution dependence, (11)–(13) also show that the coherent diffraction intensity is proportional to λ^2. This, coupled with the fact that the coherent scattering cross section for carbon scales with λ in the energy range 2–10 keV, seems to favor the use of lower-energy X-rays. However, since the photoelectric absorption cross section has a λ^3-dependence, the overall ratio of coherent scattering to photoabsorption cross section stays more or less constant in this energy range [see also the discussion on wavelength dependence in §3.4]. In practice, higher-energy X-rays are easier to use since unwanted absorptions can be minimized. A more detailed examination regarding the choice of wavelength will have to include specific beamline arrangements, specimen characteristics and desired diffraction resolution *etc.*

3.3. Required X-ray flux

With equations (11), (12) and (13) it is straightforward to evaluate the required incident photon flux $I_0\Delta t$ for a desired time-accumulated diffracted intensity $I\Delta t$ at a given diffraction resolution d. We assume that $I\Delta t = 5$ counts per pixel is a reasonable minimum signal with $I/\sigma_I = 2.24$ at the highest resolution d. For convenience, we now consider only the cases (12), when sample volume is a constant,

$$I_0\Delta t = \frac{20\pi^3}{3r_e^2 L n_0^2 d^3 f^2 \lambda^2}, \quad (15)$$

for 3D, $V = L^3$ = a constant, and, (13), when sample thickness scales with resolution d,

$$I_0\Delta t = \frac{20\pi^3}{3r_e^2 n_0^2 d^4 f^2 \lambda^2}, \quad (16)$$

for 2D, $V = L^2 d$.

As an example, for a protein sample of volume 0.1 µm × 0.1 µm × 0.1 µm and density $\rho = 1.35$ g cm^{-3} with $f \simeq Z = 6.6$ and atomic weight $A = 13$, atom number density $n_0 = \rho N_0/A = 1.35 \times 6.02 \times 10^{23}/13 = 6.25 \times 10^{22}$ atoms cm^{-3}, where N_0 is the Avogadro constant. From (15) we obtain that if a diffraction resolution $d = 1$ nm is desired using $\lambda = 1.5$ Å X-rays, then the required accumulated incident coherent X-ray photon flux is

$$I_0\Delta t = \frac{20\pi^3/3}{(2.82 \times 10^{-13})^2 \cdot 10^{-5} \cdot (6.25 \times 10^{22})^2 \cdot (10^{-7})^3 \cdot 6.6^2 \cdot (1.5 \times 10^{-8})^2} = 6.7 \times 10^{21} \text{ photons cm}^{-2} = 6.7 \times 10^{13} \text{ photons µm}^{-2}.$$

3.4. Required X-ray dose

One can convert incident photon flux into required dose, which is defined as absorbed energy per unit mass in a specimen,

$$\text{Dose} = (I_0 \Delta t)\mu E/\rho, \tag{17}$$

where ρ is the density, μ is the linear absorption coefficient and E is the X-ray energy. Equation (17) shows that the required dose is independent of X-ray wavelength λ since, according to (15), $I_0\Delta t$ scales as λ^{-2}, E as λ^{-1} and μ as λ^{-3} (if discontinuous effects owing to absorption edges are ignored). Using the above example, and assuming a mass absorption coefficient $\mu/\rho = 4.26\ \text{cm}^2\ \text{g}^{-1}$ for C at 8 keV, the required dose for obtaining a sufficient scattering signal at 1 nm resolution is given by

$$\begin{aligned}\text{Dose} &= 6.7 \times 10^{21} \times 4.26 \times 8000 \times 1.6 \times 10^{-19} \times 10^3 \\ &= 3.6 \times 10^{10}\ \text{Gy},\end{aligned}$$

which is a large radiation dose for a biological specimen.

In Fig. 3 we show the required X-ray dosage to achieve $I\Delta t$ = 5 counts per pixel as a function of diffraction resolution for a 0.1 µm × 0.1 µm × 0.1 µm biological sample (carbon, ρ = 1.35 g cm^{-3}), with minimum oversampling as defined in (8). The curves show power-law behaviors as discussed in the previous section, with a slight deviation at high resolutions owing to the effect of atomic form factor. Also plotted are the X-ray doses used in a few studies in the literature on biological specimens, which are in general agreement with our requirement curves.

Fig. 4 shows the same required dose *versus* resolution curves for an inorganic specimen of gold (ρ = 19.7 g cm^{-3}), with volumes V = 10 nm × 10 nm × d (2D case, thin solid curve) and V = 10 nm × 10 nm × 10 nm (3D case, thick solid curve). Several cases reported in the literature, plus a new simulation result discussed in §4, are shown by the filled circles in Fig. 4, again in agreement with our estimated dose requirement.

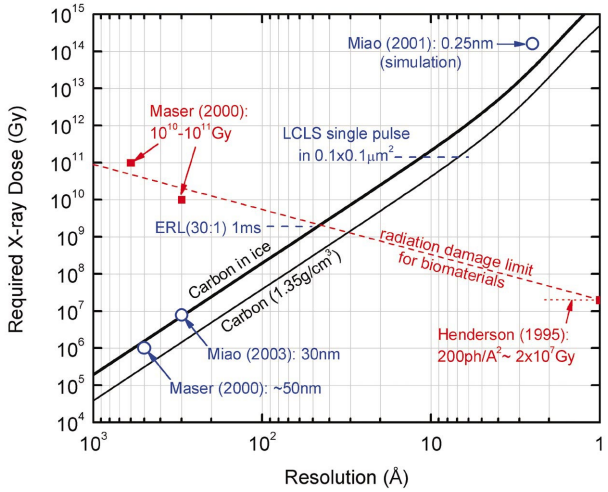

Figure 3
Required X-ray dose at 8 keV to achieve a given diffraction resolution for biological samples in ice (thick solid line) and in a vacuum (thin solid line). A fixed sample volume of V = 0.1 µm × 0.1 µm × 0.1 µm is assumed. Also plotted are several studies in the literature. The radiation-damage limit is shown as the dotted line connecting Henderson's limit at atomic resolution and microscopy studies against mass loss at low resolutions. Dose levels of proposed ERL and XFEL sources are also indicated in the plot. See text for more details.

3.5. Effect of radiation damage

Radiation damage is a critically important issue in high-resolution diffraction imaging of biomaterials with synchrotron X-rays. Several studies have shown that radiation-damage effects in biological specimens at a given dose level depend on the spatial resolution of interest. At atomic resolution it is commonly accepted (Henderson, 1995) that a dose of 2 × 10^7 Gy would be enough to destroy crystalline orders in protein crystals. At much lower resolutions, however, soft X-ray microscopic studies of mass losses in biological specimens have shown that much higher X-ray dosages of 10^{10}–10^{11} Gy can be tolerated at cryotemperatures (Maser *et al.*, 2000). A dotted straight line connecting these two extreme cases is shown in Fig. 3 as a simple-minded guideline to the radiation-damage limit at different spatial resolutions. It shows that in a continuous-wave imaging experiment with X-rays, radiation damage would limit the spatial resolution to about 5 nm for biomaterials in ice and to about 3 nm for biomaterials in a vacuum.

It may be noted that the radiation-damage limit shown in Fig. 3 is purely empirical, and is for biological specimens only. For inorganic materials the radiation tolerance may be much higher. For example, based on electron microscopy observations, the damage dose level to carbon nanotubes can be 10^2 times higher than that to biological materials (Zuo *et al.*, 2003). This fact, together with a higher density, would allow much higher spatial resolution, perhaps approaching atomic resolution, for coherent diffraction imaging of inorganic materials.

4. Simulated case study

It is important to verify that a minimally oversampled diffraction pattern with minimally satisfied X-ray intensity requirement can in fact be analysed to faithfully recover the original real-space object using the iterative phasing method. In order to test this, we have performed computer simulations of a coherent diffraction pattern on a 2D object, as shown in Fig. 5. The object consists of 2894 gold atoms located in a 10 nm cube, arranged in such a way that its 2D projection along the z-axis exhibits the pattern in Fig. 5(b). The coherent diffraction pattern from such an object, shown in Fig. 5(a), is calculated using equation (1), with incident coherent X-ray flux I_0 = 3 × 10^{14} photons s^{-1} µm^{-2} at an X-ray wavelength λ = 1.5 Å. This

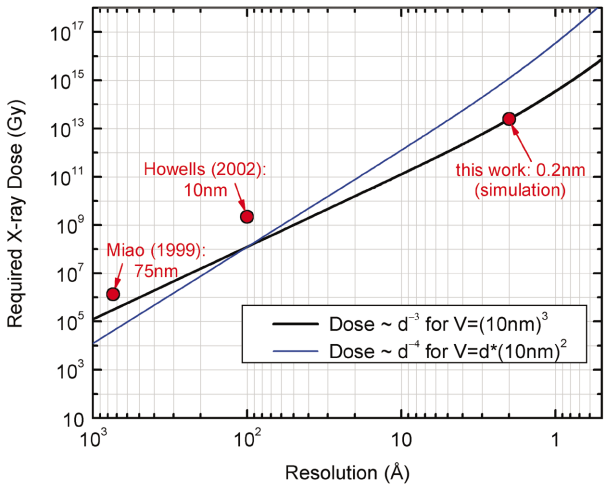

Figure 4
Required 8 keV X-ray dose as a function of diffraction resolution for gold samples in 2D (thin solid curve) and 3D (thick solid curve). The sample volume is indicated in the legend. Also plotted are several studies in the literature, plus our simulation results described in §4.

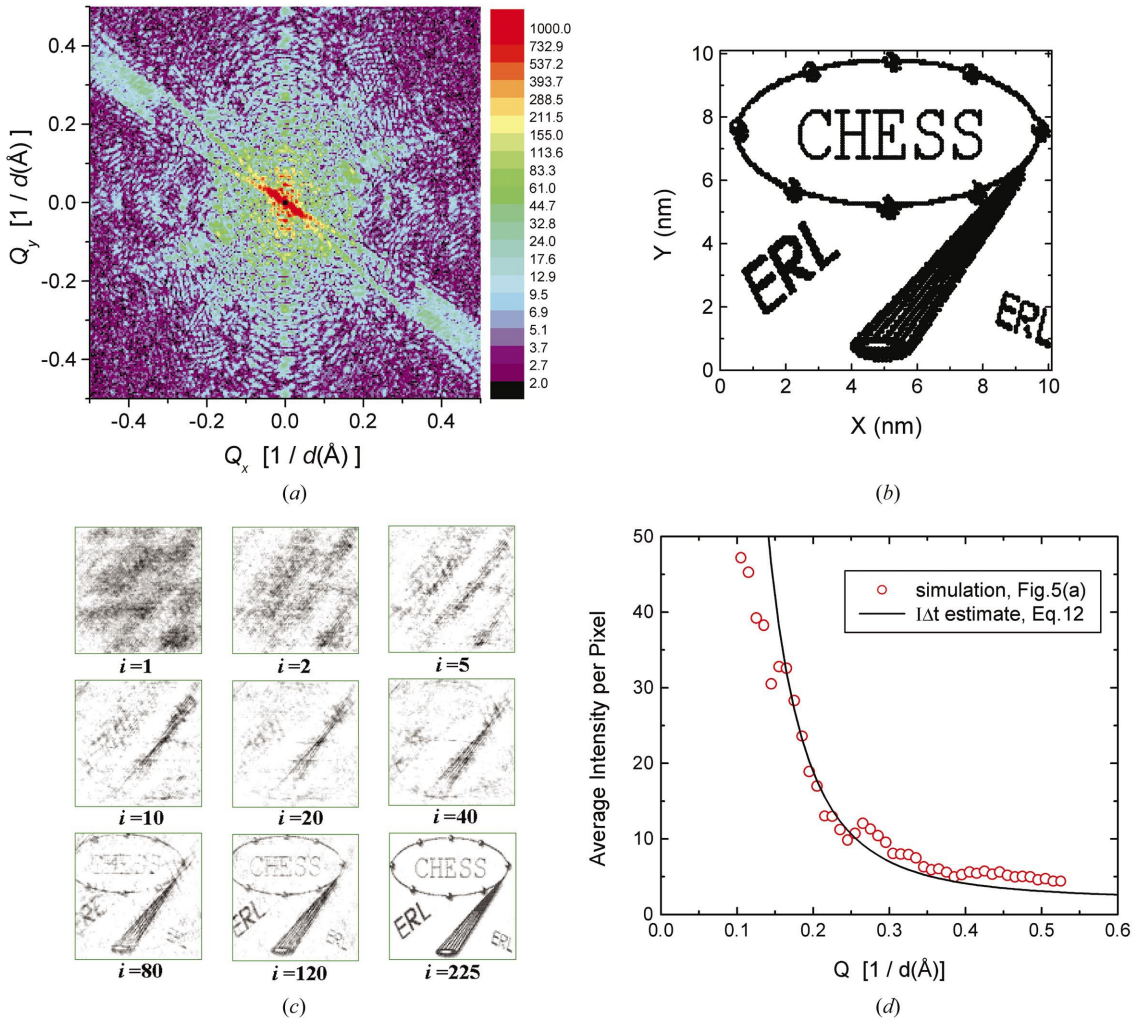

Figure 5
(*a*) Simulated coherent X-ray diffraction pattern of a 2D object made of 2894 gold atoms in a 10 nm by 10 nm square, as shown in (*b*), with an oversampling ratio of 2 × 2 on a CCD detector with 255 × 255 pixels located at 10 cm from the sample. The incident coherent intensity is assumed to be a 30:1 doubly focused ERL high-coherence beam with 3×10^{14} photons s^{-1} μm^{-2}. Diffracted intensities are shown on a logarithmic scale (color bar on right-hand side) and the counting time is 4 s. Statistical noise is included in the intensity signal at each pixel. (*c*) Examples of real-space images retrieved using the iterative phasing method, with labels showing the number of iterations in each image. (*d*) Azimuthally averaged coherently scattered intensity per pixel in the simulated diffraction pattern (*a*) as a function of Q, compared with the estimated intensity per pixel using equation (12).

corresponds to a 30:1 doubly focused beam from the proposed ERL source. An oversampling solid angle $\Delta\Omega = (\lambda/2L)^2$ is used in the calculation. The structure factor $F(\mathbf{Q})$ is given by a coherent superposition of scattering amplitudes from all 2894 atoms in the sample (at $Q_z = 0$),

$$F(\mathbf{Q}) = \sum_j f_j \exp(iQ_x x_j + iQ_y y_j), \tag{18}$$

where f_j is the atomic scattering factor for the jth gold atom located at (x_j, y_j). In our case, all f_j values are the same, and are calculated using the published values in *International Tables for Crystallography* (2001). The final intensity at each pixel is evaluated for a data-acquisition time of $\Delta t = 4$ s, plus a constant dark-current background of 2 counts per pixel, and includes a statistical noise within plus or minus one standard deviation. Furthermore, the 3 × 3 pixels at the center of the diffraction pattern are assumed to be blocked by a beam stop. The total dose accumulated in the specimen is 3×10^{13} Gy.

The simulated diffraction pattern, shown in Fig. 5(*a*), is then used as the input to a phase-retrieval computer program based on the difference-map iterative algorithm developed by Elser (2003). Starting from a random density, the algorithm updates this object by adding, in each cycle, the difference of two modifications. In one modification the object is minimally changed to agree with the measured diffraction data. The other modification reflects the knowledge about the extent of the object and sets the contrast to zero in the region not occupied by the object. When these two modifications produce the same object, their difference vanishes and the iterative updates are halted. As can be seen in Fig. 5(*c*), after some 200 iterations the real-space image retrieved using this technique is in excellent agreement with the original object, Fig. 5(*b*). The retrieved image shows that individual gold atoms can be resolved in this simulation experiment at 2 Å resolution.

The use of a focused incident X-ray beam for coherent diffraction requires some discussion. In general the convergent angle $\delta\theta$ of the incident beam should be small compared with the oversampling angular requirement. We note that a 30:1 focused ERL beam would give rise to a convergent angle $\delta\theta = 0.16$ mrad, which is much smaller than the oversampling requirement of 1.06 mrad for an object size of

100 nm. Thus the focusing should have minimal effects on our simulated diffraction pattern and the phase retrieval.

In Fig. 5(*d*) we show the azimuthally averaged intensity per pixel as a function of Q for the diffraction pattern Fig. 5(*a*). Our intensity estimate (solid curve), equation (12), agrees very well with the actual pixel intensity in the resolution range of interest. We note that (12) deviates more from the actual counts at low Q. This is due to the fact that, when the resolution (volume element) approaches the size of the specimen, (11)–(13) become invalid as I diverges at $Q = 0$. A reasonable validity requirement for these equations is that the size of the specimen should be at least ten times larger than the resolution volume element.

The X-ray dose corresponding to our simulation and phasing result is plotted in Fig. 4 at 0.2 nm resolution. We have verified that the average accumulated count at 2 Å resolution is $I\Delta t = 4.7$ photons per pixel in Fig. 5(*a*), very close to what is assumed in Fig. 4. It is interesting to note that the corresponding dose level is apparently below the minimum dose level as required by the d^{-4} scaling law based on (16) for thickness $L \propto d$.

5. Discussion and conclusions

One may ask the question of whether a larger specimen would increase the coherently scattered signal and would thus require a smaller dose to achieve the same resolution. From (10) we see that a larger volume L^3 requires a smaller oversampling solid angle which scales as L^{-2} and cancels out the factor L^2 in the increase of scattered signal. Therefore the coherently scattered intensity scales linearly with the sample thickness L, or as $V^{1/3}$, as shown in (15). It can be concluded that a larger specimen would indeed help in a coherent diffraction imaging experiment. This conclusion is consistent with, for example, Henderson (1995), where the scattered signal is shown to scale as the inverse third power of the particle size.

It remains to be seen whether the increased number of atoms or volume elements, which scales as L^3, would pose difficulties in achieving the same high-resolution real-space image in the iterative phasing procedure. For example, a macromolecular specimen of 100 nm × 100 nm × 100 nm contains roughly 6×10^7 atoms using $\rho = 1.35$ g cm^{-3}. If the volume is increased to 100 µm × 100 µm × 100 µm there would be 6×10^{16} atoms in the specimen! It would indeed be a challenge to locate all these atoms. Nonetheless, if phasing could be performed, then the lower required dose would allow higher resolution to be reached in a diffraction imaging experiment.

The effect of radiation damage in biological materials dictates the highest spatial resolution that can be achieved in a continuous-wave coherent X-ray scattering experiment, as shown in Fig. 3. In order to overcome this limit, Neutze *et al.* (2000) proposed to take advantage of the short-pulse nature of XFEL sources and to try to record a coherent diffraction pattern from single macromolecules in a single shot of a <10 fs X-ray burst. As indicated in Fig. 3, the X-ray flux from a single pulse of the LCLS source is not sufficient to provide an atomic resolution diffraction pattern, and repeated pulses have to be used to build up the statistics on a diffraction pattern from many single particles. Because each pattern is collected on a different molecule with presumably unknown orientation, millions of diffraction patterns from randomly oriented but otherwise identical molecules have to be sorted and classified. Our dose estimate results in Fig. 3 confirm that this approach may indeed be feasible, at least in principle. Fig. 3 shows that a single LCLS pulse containing 10^{12} photons may be strong enough to provide diffraction patterns at 6–12 Å resolution, which may allow proper classification and sorting of the patterns obtained on different orientations. Once these patterns are properly sorted, accumulations of the same patterns could allow structure determination at close to atomic resolution as demonstrated by Miao *et al.* (2001). Of course, many technical challenges remain to be solved for this type of experiment on single particles, and further discussion of this topic is well beyond the scope of present work.

In conclusion, we have presented a simple estimation of coherent X-ray flux and dose requirement in diffraction imaging experiments on nonperiodic specimens. Our results show that the scaling law of flux or dose *versus* spatial resolution can vary, depending on whether certain quantities are kept constant. In the most common case of a specimen with a constant volume and 3D density, we show that the required flux and dose scales as d^{-3}, or the inverse third power of spatial resolution. Based on this result and on empirical radiation-damage data in the literature, we conclude that the resolution would be limited to 3–5 nm in conventional diffraction imaging experiments on biological specimens of size 100 nm. Larger specimens would help to enhance the scattering signal and thus potentially increase the achievable spatial resolution. For radiation-resistant non-biological materials such as nanostructures and nanocomposite materials, a much higher spatial resolution, perhaps close to atomic resolution, may be obtained.

We would like thank our colleagues Sol Gruner, Don Bilderback, Ken Finkelstein and Veit Elser at Cornell, and Malcolm Howells at Lawrence Berkeley National Laboratory for useful discussions. This work is supported by the National Science Foundation and by the National Institute of General Medical Sciences through CHESS under award number DMR 0225180.

References

Arthur, J. *et al.* (2002). *Linac Coherent Light Source (LCLS) Conceptual Design Report*, http://www-ssrl.slac.stanford.edu/LCLS/CDR/.
Bilderback, D. H., Bazarov, I. V., Finkelstein, K., Gruner, S. M., Padamsee, H. S., Sinclair, C. K., Shen, Q., Talman, R., Tigner, M., Krafft, G. A. & Merminga, L. (2003). *J. Synchrotron Rad.* **10**, 346–348.
Elser, V. (2003). *J. Opt. Soc. Am.* A**20**, 40–55.
Fienup, J. R. (1982). *Appl. Opt.* **21**, 2758.
Gershberg, R. W. & Saxton, W. O. (1972). *Optik*, **25**, 237.
Gruner, S. M., Bilderback, D., Bazarov, I., Finkelstein, K., Krafft, G., Merminga, L., Padamsee, H., Shen, Q., Sinclair, C. & Tigner, M. (2002). *Rev. Sci. Instrum.* **73**, 1402–1404.
He, H., Marchesini, S., Howells, M., Weierstall, U., Hembree, G. & Spence, J. C. H. (2003). *Acta Cryst.* A**59**, 143–152.
Henderson, R. (1995). *Q. Rev. Biophys.* **28**, 171–193.
Howells, M. R., Chapman, H., Hau-Riege, S., He, H., Marchesini, S., Spence, J. & Weierstall, U. (2003). *J. Phys. IV*, **104**, 557–561.
International Tables for Crystallography (2001). Volume B. Dordrecht: Kluwer Academic Publishers.
Kirz, J., Jacobsen, C. & Howells, M. (1995). *Q. Rev. Biophys.* **28**, 33–130.
McEwen, B. F., Downing, K. H. & Glaeser, R. M. (1995). *Ultramicroscopy*, **60**, 357–373.
Marchesini, A., Chapman, H. N., Hau-Riege, S. P., London, R. A., Scoke, A., He, M., Howells, M. R., Padmore, H., Rosen, R., Spence, J. C. H. & Weierstall, U. (2003). *Opt. Express*, **11**, 2344–2353.
Maser, J., Osanna, A., Wang, Y., Jacobsen, C., Kirz, J., Spector, S., Winn, B. & Tennant, D. (2000). *J. Microsc.* **197**, 68–79.
Miao, J., Charalambous, P., Kirz, J. & Sayre, D. (1999). *Nature (London)*, **400**, 342–344.

Miao, J., Hodgson, K. O., Ishikawa, T., Larabell, C. A., LeGros, M. A. & Nishino, Y. (2003). *Proc. Natl Acad. Sci. USA*, **100**, 110–112.
Miao, J., Hodgson, K. O. & Sayre, D. (2001). *Proc. Natl Acad. Sci. USA*, **98**, 6641–6645.
Miao, J., Ishikawa, T., Johnson, B., Anderson, E. H., Lai, B. & Hodgson, K. O. (2002). *Phys. Rev. Lett.* **89**, 088303.
Miao, J., Sayre, D. & Chapman, H. N. (1998). *J. Opt. Soc. Am.* A**15**, 1662–1669.
Neutze, R., Wouts, R., Spoel, D., Weckert, E. & Hajdu, J. (2000). *Nature (London)*, **406**, 752–757.
Sayre, D. (1980). *Imaging Processes and Coherence in Physics*, edited by M. Schlenker. Berlin: Springer-Verlag.
Sayre, D. (2002). *Struct. Chem.* **15**, 81–96.
Shen, Q. Bilderback, D. H., Finkelstein, K. D., Bazarov, I. V. & Gruner, S. M. (2003). *J. Phys. IV*, **104**, 21–25.
Warren, B. E. (1969). *X-ray Diffraction.* Reading, MA: Addison-Wesley.
Williams, G. J., Pfeifer, M. A., Vartanyants, I. A. & Robinson, I. K. (2003). *Phys. Rev. Lett.* **90**, 175501.
Zuo, J. M., Vartanyants, I., Gao, M., Zhang, R. & Nagahar, L. A. (2003). *Science*, **300**, 1419–1421.

 Received 4 May 2004 • Accepted 8 July 2004